*Progress In Electromagnetics Research M, Vol. 113, 35–45, 2022*

# A Microwave Displacement Sensor Based on SIW Double Reentrant Cavity with Ring Gaps

**Jixu Ma, Yukang Chen, and Jie Huang***

**Abstract**—In this study, a double reentrant cavity sensor (DRECS) loaded with ring gaps is proposed to characterize the displacement that the metal plate is inserted into the DRECS. The conventional substrate-parasitic-capacitance of DRECS in the substrate integrated waveguide (SIW) configuration, which has no contribution to the sensitivity, is successfully eliminated by using a symmetric double reentrant cavity. The ring gaps are introduced in SIW DRECS to effectively suppress the fringe electric field around the post and enlarge the range of displacement measurements. Additionally, a displacement model, which is characterized by the quantitative relationship between the resonant frequency of DRECS and insertion depth inside DRECS, is theoretically established with the help of the electric field distribution and the equivalent circuit of the DRECS. A prototype of the designed sensor is fabricated and measured. The sensor work at 1.5–3.1 GHz and the measured results are in good agreement with the simulated ones from the displacement model. The measurement results indicate that the sensor has a displacement test range of 27 mm and $Q$-factor of over 150, and can achieve high sensitivity of 58 MHz/mm.

## 1. INTRODUCTION

In recent years, due to the important role of displacement sensors in liquid level detection, bridge gap detection, elevator position control system, robot control, and other industrial modernization fields [1], various types of displacement sensors have emerged. The microwave sensors are also widely studied for displacement sensing because of their compact structure, high sensitivity, and easy integration. Microwave sensors due to these advantages are used in many fields, such as identification of edible oil species [2], detecting and classifying transition metals [3], pest detection [4], and angular displacement measurement [5]. Various microwave resonators, including SRRs [6, 7], defected ground structure (DGS) [8], complementary split-ring resonator (CSRR) [9], and resonant cavity [10], are used in the design of displacement sensors. For example, in the work [6], the symmetry property of SRRs is used for displacement measurement. When the SSRs are moved, the symmetry of the sensor is broken, and a corresponding change in the transmission response occurs. Nonetheless, due to the short distance between the two slots of the coplanar waveguide, the measurement distance of the sensor is only 0.6 mm. The work [11] tries to adjust SRRs to diamond-shaped tapered SRRs, and only increases the measurement range to 1.2 mm. Additionally, by inserting a metal plate into a cavity, the authors proposed a displacement sensor based on a feeding structure with a rectangular open loop and a double-layer coupled SRR [1]. But the electric field decreases sharply when the double-layer structure is more than a certain distance from the feeding structure, resulting in the limitation of its distance dynamic range as well.

SIW technology benefits from its compact structure and simple fabrication, and has been used in various designs [12–14]. For instance, in the work [14] the authors replace one electrical wall of the SIW structure with open quarter guided wavelength stubs. The resonant frequency is shifted by changing

*Received 1 May 2022, Accepted 12 August 2022, Scheduled 1 September 2022*
* Corresponding author: Jie Huang (jiehuang@swu.edu.cn).
The authors are with the College of Engineering and Technology, Southwest University, Chongqing 400715, China.

the length of the stubs. Nevertheless, the length of the stubs is limited by the wavelength and cannot be higher than a quarter of the wavelength, which limits the measurement range to 15 mm. Recently, reentrant cavity sensor (RECS), which has the advantage of a highly concentrated electric field and high $Q$-factor, has been widely studied [15–17]. In the work [17], a differential RECS is proposed to measure micro-displacement, but the displacement range is only 0.4 mm. The conventional reentrant cavity also has the disadvantages of large size and high manufacturing cost, which can be solved by using SIW technology to miniaturize and planarize the cavity while maintaining the high $Q$-factor and electric field distribution characteristics of RECS [18]. However, there are few studies on the application of SIW RECS in microwave displacement sensors.

In this paper, a modified SIW DRECS for displacement sensing is proposed. The structure takes advantage of the concentrated electric field induced by the reentrant resonant cavity, and then utilizes ring gaps to obtain a higher measurement range than these reported works mentioned above, up to 27 mm while ensuring a high sensitivity. At the same time, it maintains the advantage of the high $Q$-factor of the sensor, ensuring a high resolution of the sensor. In addition, by analyzing the electric field distribution and equivalent circuit, the sensor establishes a displacement model that describes the relationship between displacement and resonant frequency of DRECS. The sensor achieves the design goal through experimental verification, providing a usable technological solution for displacement measurement in the industry.

## 2. DESIGN OF DISPLACEMENT SENSOR

### 2.1. Structure of Microwave Sensor

A displacement sensor formed by double reentrant cavity loading two ring gaps to suppress the fringe electric field around the capacitive post is proposed and shown in Fig. 1. The sensor is named ring

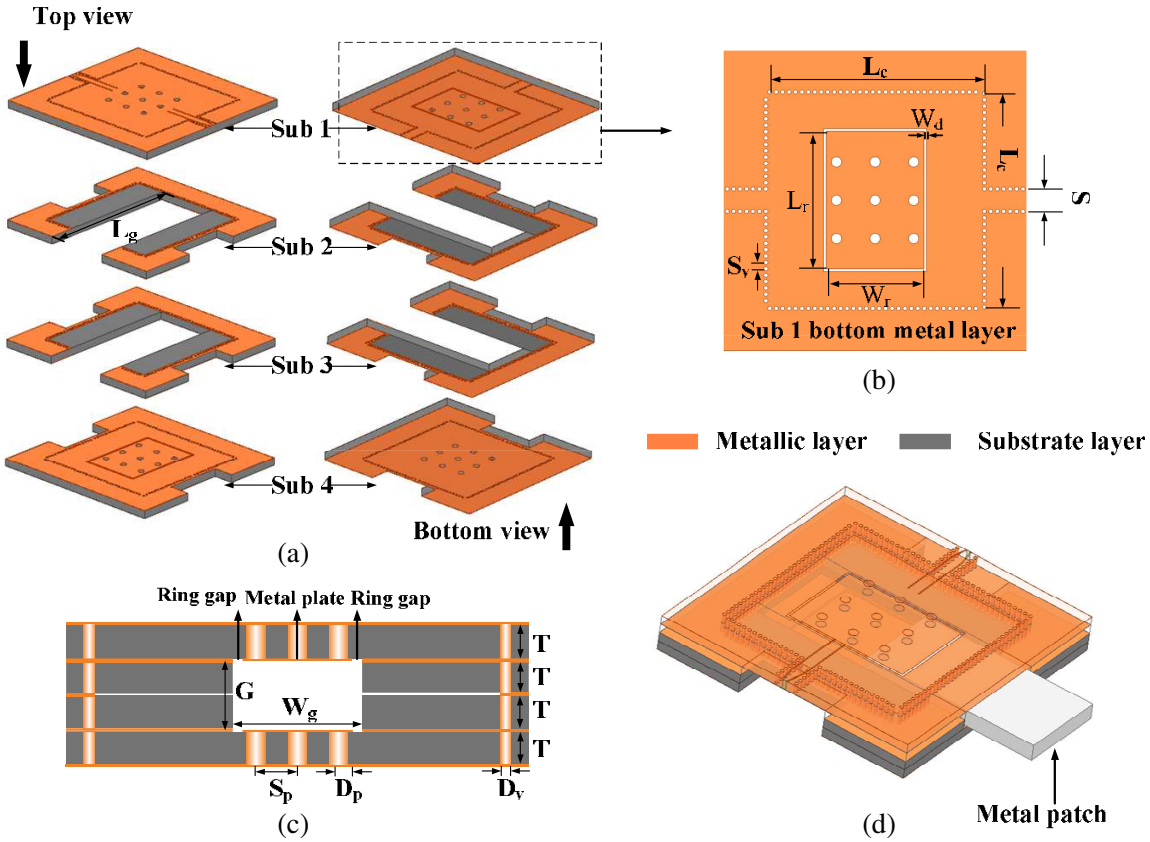


**Figure 1.** The geometry of the RG-DRECS: (a) exploded view, (b) Sub 1 bottom metal layer, (c) cross-sectional view, (d) full view.

gap loaded double reentrant cavity sensor (RG-DRECS). As illustrated in Figs. 1(a) and (c), the RG-DRECS consists of four dielectric substrates with an equal thickness of 2 mm, and the dielectric substrate is F4BM with a relative dielectric constant of 2.65 and loss tangent of 0.001. Both the top and bottom surfaces of each substrate are covered with a 35 µm metal layer. A metallized vias array is embedded in the substrate to connect the top and bottom copper films of the substrate and implement the metal cavity wall and two capacitive posts. In order to insert the movable metal patch into the cavity to perturb the electromagnetic resonant characteristics of the sensor, Sub 2 and Sub 3 are partially hollowed out from the top to the bottom metal layer. As displayed in Fig. 1(b), a ring gap is etched on the bottom and top metal layers of Sub 1 and Sub 4, respectively. Table 1 summarizes the geometric parameters of the RG-DRECS.

**Table 1.** Geometric parameters of the RG-DRECS.

| Parameter | Description | Value (mm) |
|---|---|---|
| $L_c$ | Cavity length | 42 |
| $T$ | Substrate height | 2 |
| $L_g$ | Groove length | 49.85 |
| $W_g$ | Groove width | 21 |
| $G$ | drift gap | 4.14 |
| $L_r$ | The inner length of the ring gap | 27 |
| $W_r$ | The inner width of the ring gap | 19 |
| $W_d$ | Spacing of ring gap | 0.5 |
| $S$ | Width of the CPW feedline and CPW slots | 2.31 |
| $S_p$ | Via spacing of capacitive post | 7.5 |
| $S_v$ | Via spacing of cavity wall | 1.25 |
| $D_p$ | Diameter of via of capacitive post | 2 |
| $D_v$ | Diameter of the metallized via | 0.8 |

The structure of the sensor is considered using a reentrant cavity with a highly concentrated electric field between the capacitive post and the top lid of the cavity. When a moving metal patch is inserted in this gap region of RG-DRECS, small displacements can produce relatively large variations in resonant frequency. Therefore, a groove for metal patch moving is designed that passes through this gap region. In general, greater sensitivity of the RG-DRECS can be achieved by increasing the longer depth of the groove to enhance the perturbation to the gap region, but there is inevitably a non-removable dielectric layer between the top of the groove and the bottom metal layer of the cavity. As shown in Fig. 2(a), $\varepsilon_r$ and $\varepsilon_0$ are the permittivity of substrate and permittivity of free space. The gap capacitance $C_p$ is modified to capacitance $C_{sub}$ and $C_g$ in series by the remaining dielectric layer and the groove. $C_{sub}$ is the distributed capacitance determined by the thickness and permittivity of the remaining dielectric layer, and $C_g$ is limited by the depth of the groove. The movable metal patch does not affect the capacitance $C_{sub}$, resulting in the sensor that does not take full advantage of the concentrated electric field of the structure to generate the maximum frequency shift. The DRECS displayed in Fig. 1(c) is used to solve this problem, by which the remaining substrate layer with its resulting additional capacitance is removed, and all the gap capacitance is wholly utilized to improve the sensing sensitivity.

As shown in Figs. 2(b) and (c), the electric intensity field distribution of the AS-DRECS at its resonant frequency is built and compared with the conventional DRECS. It is worth noting that, without changing the size of the metal post, adding a ring gap composed of a rectangle metal plate and an annular slot makes the range of highly concentrated electric field available for measurement become larger, and the fringe electric field around the RG-DRECS metal post is effectively suppressed by the ring gaps, forming a ring capacitance. The expansion of the concentrated electric field range can increase the measurable displacement range of the sensor, and [19] has theoretically verified that

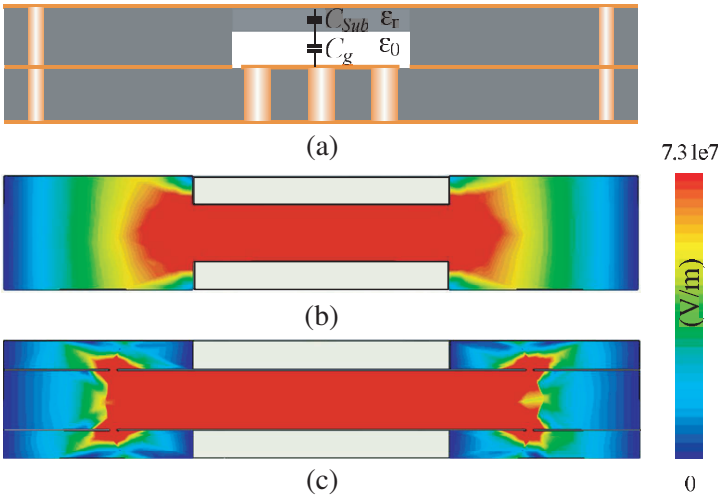


**Figure 2.** (a) Cross-sectional view of the single RECS, (b) the electric field distribution of the DRECS in the Cross-section, (c) the electric field distribution of the RG-DRECS in the Cross-section.

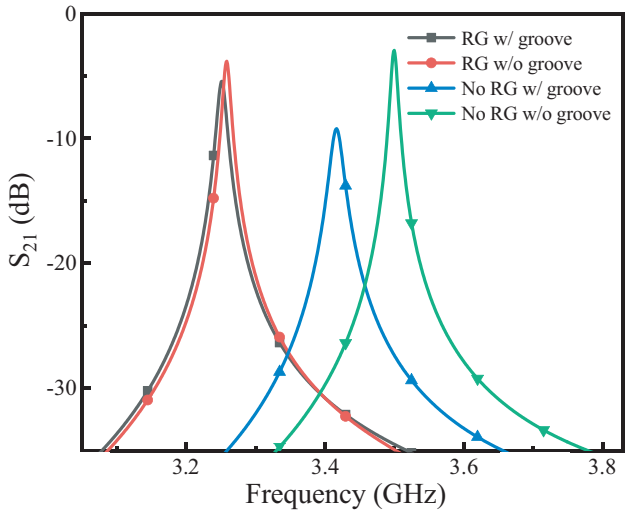


**Figure 3.** Transmission responses of RG-DRECS and DRECS before and after grooving.

the fringe capacitance determined by the fringe electric field weakens the sensitivity. The use of ring gaps also reduces the electric loss by partly grooving the substrate. Fig. 3 compares the change in the transmission responses of the sensors before and after grooving. The resonant frequency of the DRECS is reduced by 84 MHz after grooving, while the resonant frequency for the RG-DRECS is reduced by only 7 MHz after grooving.

### 2.2. Displacement Measurement Model of RG-DRECS

Figure 4(a) shows the lumped-element equivalent circuit model of the RG-DRECS, which is used to discuss a quantitative relationship between displacement distance and the resonant frequency of the RG-DRECS. $C_p$ is the gap capacitance formed between the two metal posts; $C_{r1}$ and $C_{r2}$ represent the ring capacitances formed by the ring gaps of the upper and lower reentrant cavities; $L_1$ and $L_2$ represent the equivalent inductances of the upper and lower reentrant cavities respectively; and $R$ is the equivalent resistance, which contains the total loss information of the RG-DRECS. An ideal transformer is used to represent the coupling of the RG-DRECS to the external feed line, and $n$ is the transformation ratio.

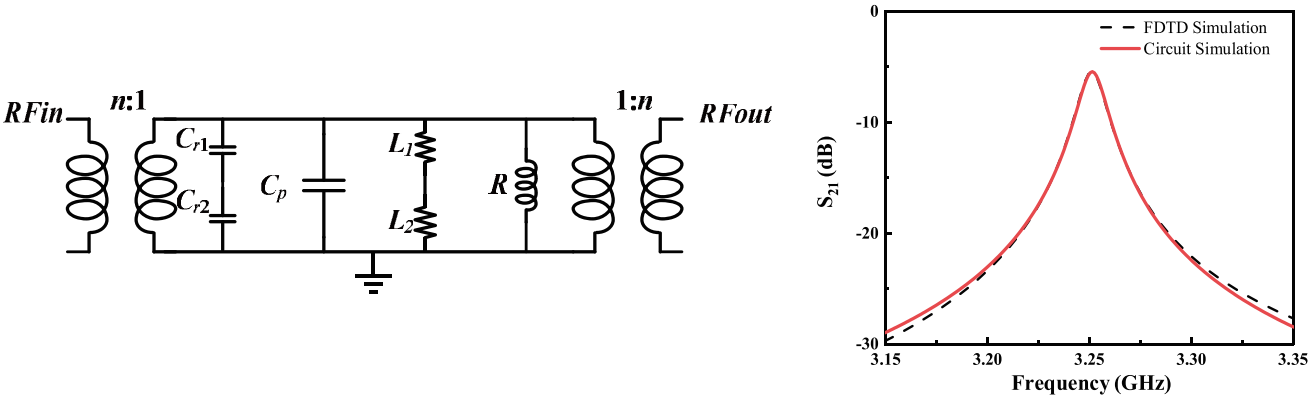


(a) (b)

**Figure 4.** (a) Equivalent lumped element circuit model of the RG-RECS, (b) the circuit and FDTD simulation result of transmission response of the RG-DRECS.

In a highly loaded cavity ($G \ll \lambda_g$, $\lambda_g$ is resonant wavelength), the electric field in the RG-DRECS gap region is close to being uniform [20], thus $C_p$ can be calculated using parallel-plate capacitance theory as Eq. (1):

$$C_p = \frac{\varepsilon_0 W_r L_r}{G} \tag{1}$$

The DRECS can be regarded as two single reentrant cavities cascaded back to back in series, so the series-parallel relationship between the equivalent inductance and the gap capacitance with the unloaded DRECS in the circuit can be determined. For a cylindrical reentrant cavity, the equivalent inductance can be obtained by coaxial transmission line theory, but for the rectangular reentrant cavity of this design, the calculation needs some modification [21]. $A$ is a factor with a value of 0.95, used to minimize the error when parameters are calculated using coaxial line transmission theory, and $\mu_0$ represents the permeability of free space. The formula is as Eqs. (2)–(3):

$$R_1 = A\sqrt{L_p^2/\pi}, \quad R_2 = A\sqrt{L_c^2/\pi} \tag{2}$$

$$L_1 = \frac{\mu_0 T}{2\pi} \ln \frac{R_2}{R_1}, \quad L_2 = \frac{\mu_0 T}{2\pi} \ln \frac{R_2}{R_1} \tag{3}$$

The ring capacitance is formed by the ring gap, which is in analogy with the standard ring gap in [22]. A correction factor $B$ needs to be used. The equivalent capacitance obtained from the rectangular ring gap of this work is obtained as Eq. (4). $\varepsilon_{r1}$ and $\varepsilon_{r2}$ represent the dielectric constant of the substrates above and below the metal layer where the ring gap is located with values of 1 and 2.65, respectively. The resonance frequency of the RG-DRECS is finally obtained as Eq. (5):

$$C_r = 2B\varepsilon_0 \left(W_r + L_S\right)\left(\varepsilon_{r1} + \varepsilon_{r2}\right) \tag{4}$$

$$f_r = \frac{1}{2\pi\sqrt{\left(L_1 L_2 / \left(L_1 + L_2\right)\right)\left(C_{r1} C_{r2} / \left(C_{r1} + C_{r2}\right)\right) + C_p}} \tag{5}$$

$$\frac{1}{Q_L} = \frac{1}{Q_0} + \frac{1}{Q_E} \tag{6}$$

To maintain electromagnetic energy in the cavity, the RG-DRECS is connected to some external circuits called feeding or coupling, which causes an offset from its desired frequency and unload quality factor $Q_0$. The offset has a correspondence with loaded quality factor $Q_L$ and external circuitry quality factor $Q_E$, as shown in Eq. (6). Through the definition formula of each quality factor and the $S$-parameter transmission matrix, and the values of $S_{21}$ and $Q_L$ obtained using Finite Difference Time Domain (FDTD) simulation, the values of $R$ and $n$ can be obtained [23, 24]. In order to acquire the simulated transmission response of the RG-DRECS by the equivalent circuit model, the specific parameters of the

**Table 2.** Value of equivalent lumped element circuit components.

| Component | $C_p$ (pF) | $C_{r1}$ (pF) | $C_{r2}$ (pF) | $L_1$ (nH) | $L_2$ (nH) | $R$ (kΩ) | $n$ |
|---|---|---|---|---|---|---|---|
| Value | 1.097 | 4.428 | 4.428 | 0.3618 | 0.3618 | 7.5007 | 0.0619 |

RG-DRECS are brought into the formula in Table 1. It is worth noting that the correction factor $B$ of Eq. (4) can be optimized and modified by Keysight ADS circuit simulation to obtain a specific value of 1.49. The specific values of all circuit components are displayed in Table 2.

The reliability of the constructed equivalent circuit model can be demonstrated by the good agreement between the FDTD simulation and circuit model simulation, as shown in Fig. 4(b), which shows that the proposed equivalent lumped element circuit model can be used to investigate the relationship between the displacement and resonant frequency of the RG-DRECS to attain the displacement measurement model in the following sections.

The movement of the movable metal patch in the RG-DRECS will perturb the electric field in the gap region. In the gap region, the electric field distribution varies along with the movement of the movable metal patch, resulting in resonant frequency shifts. This variation can be used to measure the value of the displacement of the movable metal patch, which can range from 0 to 27 mm. From the established equivalent lumped element circuit model and the electric field distribution of the moving metal path into the cavity shown in Fig. 5(a), it can be analyzed that the displacement of the movable metal patch changes the gap capacitance $C_p$ and divides the gap region of the resonant cavity into two parts, the electric field distribution in both parts is relatively uniform. According to the parallel plate capacitance theory, $C_p$ can be equivalently replaced by two capacitances $C_1$ and $C_2$, and the relationship between $C_1$ and $C_2$ and displacement $x$ is shown in Eqs. (7)–(8):

$$C_1 = \frac{\varepsilon_0 W_r x}{G-h} \tag{7}$$

$$C_2 = \frac{\varepsilon_0 W_r \left(L_r - x\right)}{G} \tag{8}$$

where $h$ is the height of the movable metal patch. In order to make full use of the gap region and to ensure the reliability of Eqs. (7)–(8), the width of the metal patch needs to be no less than the width of the inner width of the ring gap $W_r$. In addition, for a more intuitive analysis, as shown in Fig. 5(b), the existing equivalent circuit model is simplified and adjusted. $C_r$ is an equivalent capacitor of two ring capacitances; $L$ is the equivalent inductance of the RG-DRECS; and $C_p$ has been correspondingly modified accordingly to capacitance $C_1$ and $C_2$.

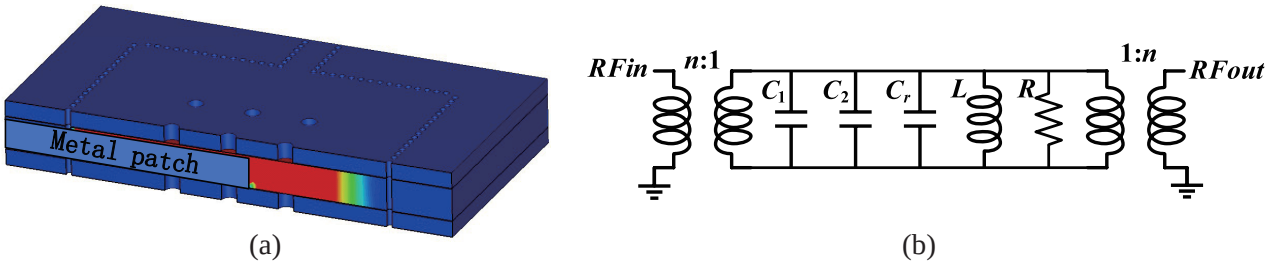


**Figure 5.** After adding the movable metal patch, (a) electric field distribution, (b) equivalent circuit model.

On the basis of the equivalent circuit model in Fig. 5(b), the relationship between the displacement $x$ of the movable metal patch and resonant frequency $f_r$ of the RG-DRECS is investigated. Using Eqs. (7)–(8) and (5), we can obtain displacement measurement model:

$$f_r = \frac{1}{2\pi\sqrt{L\left(C_r + \left(\frac{\varepsilon_0 W_r x}{G-h} + \frac{\varepsilon_0 W_r \left(L_r - x\right)}{G}\right)\right)}} \tag{9}$$

## 3. FABRICATION, MEASUREMENT AND DISCUSSION

### 3.1. Sensor Fabrication and Measurement Setup

To experimentally verify the accuracy of the displacement measuring mode for the RG-DRECS, the prototype of the RG-DRECS is fabricated by standard print circuit board (PCB) technology. The sensor consists of four substrates, and Fig. 6(a) shows the top and bottom views of each substrate of the fabricated sensor prototype, and Fig. 6(b) shows the prototype of the sensor and the overall experimental setup composed of a vector network analyzer (E5071C, Agilent, Beijing, China) and a displacement measurement platform. All measurements of resonant parameters such as transmission response and $Q$-factor are performed by the vector network analyzer (VNA), which is connected to the sensor through a pair of coaxial cables. The metal patch is fixed to a spiral micrometer that can move one-dimensional movement manually, with a measurement range of 0–27 mm and testing accuracy of 100 µm.

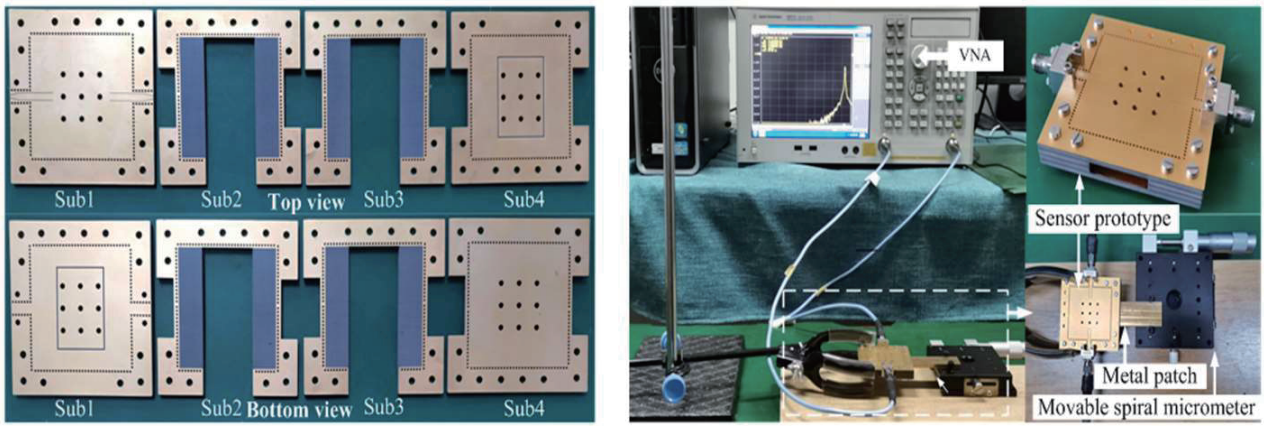


(a) (b)

**Figure 6.** Photographs of (a) the top and bottom views of each layer of the RG-DRECS, (b) displacement measurement setup.

To ensure the accuracy of the experiment, the VNA is calibrated before the measurement using standard calibration kit 85052D to eliminate some systematic errors. The spiral micrometer is fixed on a smooth wooden board, and the sensor prototype is held in place by clamps to the flatter displacement system. When the measurement is started, the relative displacement of the metal patch and RG-DRECS prototype can be generated by the accurate one-dimensional movement of the spiral micrometer, and the transmission responses at different displacements are recorded by the VNA to obtain the relationship between the actual displacement and resonant frequency of the RG-DRECS.

### 3.2. Results and Discussions

It can be seen that the thickness of the metal path affects the relationship between the displacement $x$ and resonant frequency $f_r$ from Eq. (9), and Fig. 7 depicts the measured transmission responses $S_{21}$ of the RG-DRECS at different displacements when the thickness of the metal patch is 3.64 mm. From Fig. 7(a), we can notice that when the displacement gradually increases from 0 mm to 27 mm, the resonant frequency drops from 3.1 GHz to 1.5 GHz, and this situation is consistent with the displacement mechanism analyzed above. Fig. 7(b) shows the measured transmission responses $S_{21}$ of the sensor for displacements in the range from $x = 0$ µm to $x = 1000$ µm in steps of 200 µm, which demonstrates a relatively high resolution.

The correspondence between resonant frequency and the displacement of metal patches with different thicknesses is illustrated in Fig. 8(a) (measured results are the average value of four measurements). It can be shown from Fig. 8(a) that the displacement model established by Eq. (9) is

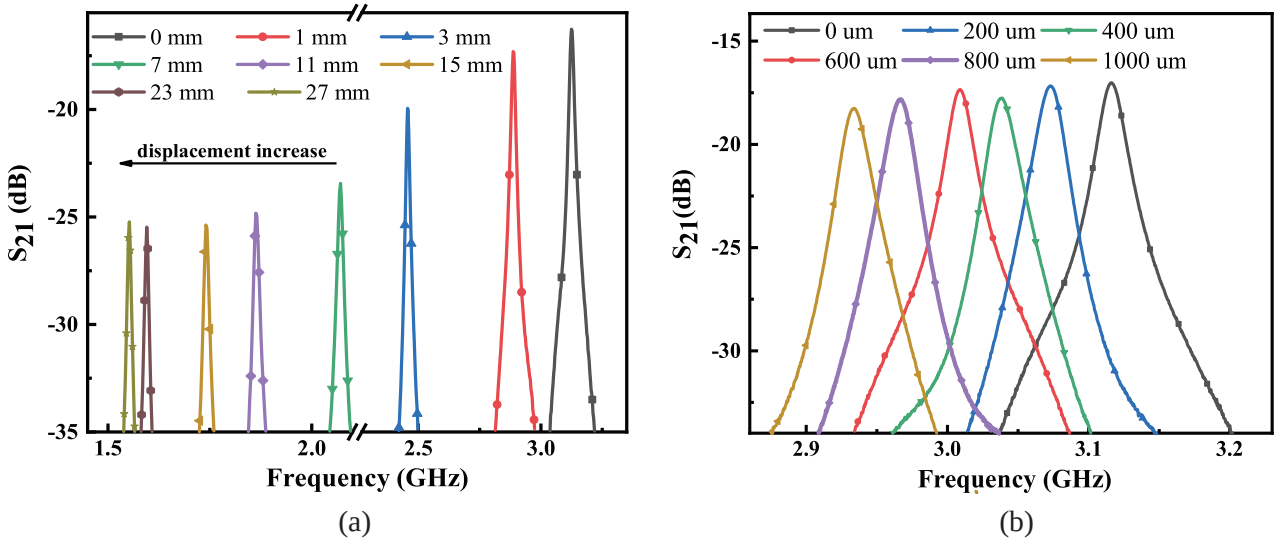


**Figure 7.** Different displacements correspond to the measured transmission responses when the thickness of the metal patch is 3.64 mm, (a) 0–27 mm, (b) 0–1 mm.

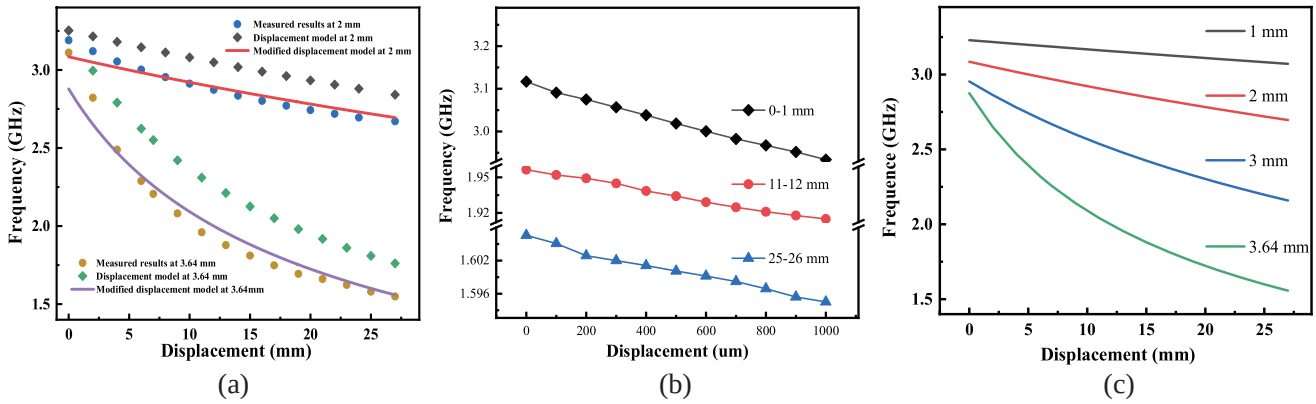


**Figure 8.** (a) The correspondence between resonant frequency and the displacement of metal patches with different thicknesses, (b) resonant frequency of the fabricated sensor at different displacement $x$ values when the thickness of the metal patch is 3.64 mm, (c) correspondence between displacement and resonant frequency at different thicknesses obtained by modified displacement model.

approximate to the variation trend of the measured results, but there is a certain deviation, which may be caused by the fact that the metal patch cannot fit closely to the bottom of the groove [1], and the metal patch reflects the electromagnetic energy to the external environment. To make the model more accurate, Eq. (9) needs to be revised. By using two sets of measured data with metal patch thicknesses of 2 mm and 3.64 mm and curve fitting, the modified displacement model is established:

$$f_r = \frac{1}{2\pi\left(47 * h + 0.96\right)\sqrt{L\left(C_r + \left(\frac{\varepsilon_0 W_r x}{G} - h + \frac{\varepsilon_0 W_r \left(L_r - x\right)}{G}\right)\right)}} \tag{10}$$

Fig. 8(a) shows that the modified displacement model has a good approximation with the measured results for different thicknesses of metal patches, which proves the reliability of the model. In addition, to experimentally verify the resolution of the RG-DRECS, a micro-displacement test with a step size of 100 μm is conducted at different intervals within the test range of the sensor, and the results are shown in Fig. 8(b), which shows that the sensor has a high resolution.

The average sensitivity of the displacement sensor can be deduced from the following formula:

$$S=\frac{|\Delta f_r|}{|\Delta x|} \tag{11}$$

where $\Delta f_r$ is the difference between the maximum and minimum resonant frequencies in the displacement range, and $\Delta x$ is the difference between the maximum and minimum displacements in the displacement range. The maximum displacement range $\Delta x$ of the sensor is 27 mm, which is the inner length of the ring gap $L_r$. In addition, Eq. (10) indicates the correspondence between the displacement of the metal patch and the resonant frequency, and the thickness $h$ of the metal patch is one of the important parameters. Setting $h$ in Eq. (10) as a variable parameter, as shown in Fig. 8(c), in the case of the maximum displacement range $\Delta x$ is $L_r$. The larger the $h$ is, the larger the resonant frequency shift $|\Delta f_r|$ is, and the higher the sensitivity $S$ of the sensor is. Meanwhile, from the measured results, reducing the thickness of the metal patch can improve the linearity of the displacement correspondence, which is shown in Fig. 8(a).

According to Fig. 8, the sensor provides a high measurement range while ensuring a high sensitivity, and thanks to the characteristics of the structure, the sensor has a high $Q$-factor, which guarantees the resolution of the sensor [25]. In addition, although the dynamic displacement range of all tests is 0–27 mm, it can be analyzed from the above measured results that other characteristics of the RG-DRECS are affected by the thickness of the metal patch. In practical applications, different thicknesses of the metal patch can be selected according to the requirements of sensitivity, linearity, and $Q$-factor to achieve the desired sensor performance. Table 3 provides a comparison between the designed sensor and other recently reported displacement sensors, including dynamic, sensitivity, and $Q$-factor. As seen in Table 3, 2 mm and 3.64 mm represent different metal patch thicknesses, respectively. The sensor proposed here has a great dynamic displacement measurement range, a high $Q$-factor, and good sensitivity.

**Table 3.** Comparison of the proposed sensor with the previous 1-D displacement sensors.

| Ref. | | Frequency, GHz | Size, mm | Dynamic, mm | Sensitivity | $Q$-factor | Sensor type |
|---|---|---|---|---|---|---|---|
| [1] | | 0.3–0.7 | 40 × 40 | 9 | 0.03 GHz/mm | 9 | SRRs |
| [8] | | 3–5 | 42.8 × 26.1 | 3 | 0.41 GHz/mm | 34 | DGS |
| [11] | | 1–2 | 30.3 × 15.3 | 1.2 | 21 dB/mm | 19 | SRR |
| [14] | | 2.4–2.9 | 80 × 50 | 15 | 0.026 GHz/mm | 65 | SIW |
| [26] | | 1.6–4.2 | 7.5 × 7.5 | 5 | 0.5 GHz/mm | 226 | DSRR |
| This work | 2 mm* | 2.6–3.1 | 42 × 42 | 27 | 0.019 GHz/mm | 210 | DREC |
| | 3.64 mm* | 1.5–3.1 | 42 × 42 | 27 | 0.058 GHz/mm | 155 | DREC |

* 2 mm and 3.64 mm represent the performance of the sensor with metal patch thickness of 2 mm and 3.64 mm, respectively.

## 4. CONCLUSION

In this paper, a microwave displacement sensor based on an adjusted SIW reentrant cavity is demonstrated numerically and experimentally, which consists of a double reentrant cavity and ring gaps. The purpose of the double reentrant cavity is to improve the sensitivity, and the ring gaps suppress the fringe electric field and expand the concentrated electric field region used to test the displacement. Then, the equivalent circuit model is theoretically established to reveal the relationship between displacement and capacitance variation, and a displacement measurement model of displacement and resonance frequency is obtained. This model can better explain the relationship between displacement and resonant frequency, unlike the physical-meaningless mathematical fitted one. Verified by experiment, the sensor operates in the frequency range of 1.5–3.1 GHz, provides a dynamic range of 27 mm, has a high $Q$-factor and good sensitivity, and the measurement results are in good agreement with the

displacement measurement model, which is favorable for the application of this sensor to many high-precision industrial measurement sites.

## ACKNOWLEDGMENT

This work was supported by the National Natural Science Foundation of China under Grant 61971358.

## REFERENCES

1. Wang, Y. D., F. Y. Han, J. Zhao, Z. W. Zhang, D. Wang, Y. H. Tan, and P. K. Liu, "Design of double-layer electrically extremely small-size displacement sensor," *Sensors*, Vol. 21, 4923, 2021.
2. Huang, J., J. Li, G. Xu, and Z. Wei, "A microfluidic sensor based on meta-surface absorber for rapidand nondestructive identification of edible oil species," *Progress In Electromagnetics Research C*, Vol. 96, 153–163, 2019.
3. Al-Duhni, G. and N. Wongkasem, "Metal discovery by highly sensitive microwave multi-band metamaterial-inspired sensors," *Progress In Electromagnetics Research B*, Vol. 93, 1–22, 2021.
4. Bait-Suwailam, M. M., "Numerical assessment of red palm weevil detection mechanism in palm trees using CSRR microwave sensors," *Progress In Electromagnetics Research Letters*, Vol. 100, 63–71, 2021.
5. Teng, C., C. H. Chio, K. W. Tam, and P. Y. Lau, "An angular displacement microwave sensor with 360° dynamic range using multi-mode resonator," *IEEE Sensors Journal*, Vol. 21, No. 3, 2899–2907, February 1, 2021.
6. Naqui, J., M. Durán-Sindreu, and F. Martín, "Novel sensors based the symmetry properties of Split Ring Resonators (SRRs)," *Sensors*, Vol. 11, 7545–7553, 2011.
7. Naqui, J., M. Durán-Sindreu, and F. Martín, "Alignment and position sensors based on split ring resonators," *Sensors*, Vol. 12, 11790–11797, 2012.
8. Rezaee, M. and M. Joodaki, "Two-dimensional displacement sensor based on CPW line loaded by Defected Ground Structure (DGS) with two separated transmission zeroes," *IEEE Sensors Journal*, Vol. 17, No. 4, 994–999, February 15, 2017.
9. Saadat-Safa, M., V. Nayyeri, M. Khanjarian, M. Soleimani, and O. M. Ramahi, "A CSRR-based sensor for full characterization of magneto-dielectric materials," *IEEE Transactions on Microwave Theory and Techniques*, Vol. 67, No. 2, 806–814, February 2019.
10. Soltan, A., R. A. Sadeghzadeh, and S. Mohammad-Ali-Nezhad, "Angular displacement sensor based on Corrugated Substrate Integrated Waveguide (CSIW)," *IETE Journal of Research*, August 13, 2020.
11. Horestani, A. K., C. Fumeaux, D. Abbott, et al., "Displacement sensor based on diamond-shaped tapered split ring resonator," *IEEE Sensors Journal*, Vol. 13, No. 4, 1153–1159, April 2013.
12. Salim, A., S.-H. Kim, J. Y. Park, and S. Lim, "Microfluidic biosensor based on microwave substrate-integrated waveguide cavity resonator," *Journal of Sensors*, 1–13, 2018.
13. Chen, C.-M., J. Xua, and Y. Yao, "Fabrication of miniaturized CSRR-loaded HMSIW humidity sensors with high sensitivity and ultra-low humidity hysteresis," *Sensors and Actuators B: Chemical*, 1100–1106, 2018.
14. Soltan, A., R. A. Sadeghzadeh, and S. Mohammad-Ali-Nezhad, "High sensitivity simple structured displacement sensor using Corrugated Substrate-Integrated Waveguide (CSIW)," *IET Microwaves, Antennas & Propagation*, Vol. 14, 414–418, 2020.
15. Xi, W., W. R. Tinga, W. A. Geoffrey Voss, and B. Q. Tian, "New results for coaxial re-entrant cavity with partially dielectric filled gap," *IEEE Transactions on Microwave Theory and Techniques*, Vol. 40, No. 4, 747–753, 1992.
16. Murugkar, A., R. Panigrahi, and K. J. Vinoy, "A novel approach for high Q microwave re-entrant cavity resonator at S-band," *Proceedings of the Asia-Pacific Microwave Conference*, 1–4, December 2016.

17. Asua, E., V. Etxebarria, and J. Feutchwanger, "High-precision displacement sensor based on resonant cavities through an electronic interface based on Arduino," *Sensors and Actuators A: Physical*, 296–301, 2019.
18. Saeedi, S., J. Lee, and H. H. Sigmarsson, "Tunable, high-Q, substrate-integrated, evanescent-mode cavity bandpass-bandstop filter cascade," *IEEE Microwave and Wireless Components Letters*, Vol. 26, No. 4, 240–242, April 2016.
19. Chen, Y., J. Huang, Y. Xiang, L. Fu, W. Gu, and Y. Wu, "A modified SIW re-entrant microfluidic microwave sensor for characterizing complex permittivity of liquids," *IEEE Sensors Journal*, Vol. 21, No. 13, 14838–14846, July 1, 2021.
20. Wei, Z., J. Huang, J. Li, G. Xu, Z. Ju, X. Liu, and X. Ni, "A high-sensitivity microfluidic sensor based on a substrate integrated waveguide re-entrant cavity for complex permittivity measurement of liquids," *Sensors*, Vol. 18, 4005, 2018.
21. Bansiwal, A., S. Raina, K. J. Vinoy, and S. K. Datta, "Calculation of equivalent circuit parameters of a rectangular reentrant cavity for klystron," *International Journal of Microwave and Optical Technology*, Vol. 13, No. 6, 487–492, November 2018.
22. Abdelfattah, M. and D. Peroulis, "High-Q tunable evanescent-mode cavity SIW resonators and filters with contactless tuners," *IEEE Transactions on Microwave Theory and Techniques*, Vol. 67, No. 9, 3661–3672, September 2019.
23. Pozar, D. M., *Microwave Engineering*, 3rd Edition, Wiley, Hoboken, NJ, USA, 2005.
24. Varshney, P. K. and M. Jaleel Akhtar, "Permittivity estimation of dielectric substrate materials via enhanced SIW sensor," *IEEE Sensors Journal*, Vol. 21, No. 10, 12104–12112, May 15, 2021.
25. Zarifi, M. H. and M. Daneshmand, "Monitoring solid particle deposition in lossy medium using planar resonator sensor," *IEEE Sensors Journal*, Vol. 17, No. 23, 7981–7988, December 1, 2017.
26. Abdolrazzaghi, M. and M. Daneshmand, "Multifunctional ultrahigh sensitive microwave planar sensor to monitor mechanical motion: Rotation, displacement, and stretch," *Sensors*, Vol. 20, 1184, 2020.